Magneto-spectroscopy of ordered arrays of magnetic semiconductor quantum wires

L. Chen[a], P.J. Klar[a,*], W. Heimbrodt[a], F. Brieler[b], M. Fröba[b,c], H.-A. Krug von Nidda[d], A. Loidl[d]

[a] *Department of Physics and Materials Science Centre, Philipps-University Marburg, Renthof 5, 35032 Marburg, Germany*
[b] *Department of Inorganic and Applied Chemistry, University of Hamburg, Martin-Luther-King-Platz 6, 20146 Hamburg, Germany*
[c] *Institute of Inorganic Chemistry, University of Erlangen-Nuremberg, Egerlandstraße 1, 91058 Erlangen, Germany*
[d] *Department of Physics, University of Augsburg, Universitätsstraße 2, 86135Augsburg, Germany*

1. Introduction

The organic-template directed synthesis of mesoporous silica in 1992 by Mobil Oil Company has opened new pathways in material design [1,2]. Depending on the synthesis conditions, highly ordered organic-template/SiO_2 superstructures can be prepared. The superstructures of these so called M41S materials are either of hexagonal (MCM-41; MCM= Mobil's Composition of Matter), cubic (MCM-48) or lamellar (MCM-50) symmetry. Removing the organic template of the three dimensional superstructures,

* Corresponding author. Tel.:+49-6421-282-1354; fax: +49-6421-282-7036.
E-mail address: klarp@mailer.uni-marburg.de (P.J. Klar).

i.e. MCM-41 and MCM-48, in a calcination process, leaves a highly ordered mesoporous SiO_2-matrix with regular wire-like pores. The pore diameters as well as the distances between neighbouring pores are only of a few nanometers and can be accurately adjusted during the synthesis process [3]. These mesoporous SiO_2-materials are ideally suited as host materials for semiconductors due to their high degree of order as well as the large band gap of the SiO_2 (which serves as a barrier material). Several semiconductor compounds, e.g. CdS [4], CdSe [5], GaAs [6], InP [7], Ge [8], SiGe [9], have been implantated into MCM-41 SiO_2 so far to obtain regular arrays of quantum wires. Recently, we reported on the first successful incorporation of the semimagnetic semiconductor $Cd_{1-x}Mn_xS$ into MCM-41 SiO_2 [10] and pointed out that this is an alternative way of creating highly ordered arrays of magnetic quantum wires for possible applications in magneto-electronics.

2. Experimental details

A gel mixture of 1 SiO_2 : 0.25 CTABr : 0.2 TMAOH : 35 H_2O was used for the synthesis of the MCM-41 SiO_2 matrix. The gel mixture was stirred at 60°C for 30 min. It was filled into a teflon-lined steel autoclave and kept there at room temperature for 24 h. Afterwards it was synthesised for 24 h at 150°C under autogeneous pressure. The product was washed with water several times and calcined at 550°C. The pore size and the wall thickness were determined to be 3.1 ± 0.1 nm and about 2 nm, respectively. The $Cd_{1-x}Mn_xS$ was implanted into MCM-41 SiO_2 matrix as follows: 0.5 g calcined MCM-41 silica was suspended in a 0.5 molar solution of cadmium acetate and manganese acetate in water with different ratios of Cd/Mn, and stirred for 10 min. The precipitate was centrifuged and vacuum dried. The acetates were converted into the sulphide by thermal treatment in a H_2S atmosphere. Samples with Mn-contents x of 1.5%, 5%, 9%,14% and 20% were synthesised. In a similar fashion, $Cd_{1-x}Mn_xS$ can be incorporated into cubic MCM-48 SiO_2 matrices. Fig. 1 shows a transmission electron microscopic image of a grain of MCM-48 SiO_2 before incorporation of the semiconductor. The samples were studied at liquid helium temperatures by photoluminescence (PL) and photoluminescence excitation (PLE) spectroscopy in magnetic fields up to 7.5 T as well as by electron paramagnetic resonance (EPR) spectroscopy using X-band frequencies (9.48 GHz).

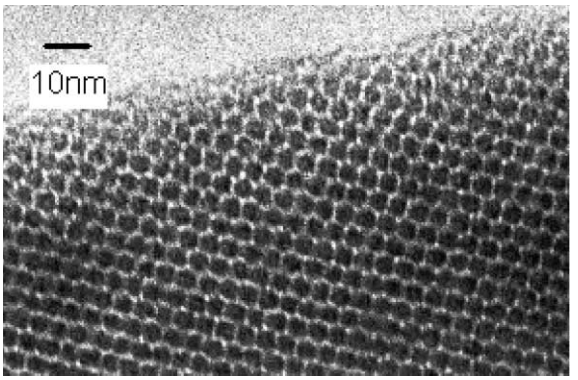

Fig. 1. High-resolution transmission electron microscopic image of the surface of a grain of the MCM-48 SiO_2 matrix material before incorporation of the semiconductor.

3. Results and discussion

Fig. 2 shows EPR spectra of five $Cd_{1-x}Mn_xS$ in MCM-41 SiO_2 powder samples with x=1.5%, 5%, 9%, 14% and 20%, respectively. All spectra were taken at 4 K and normalised to the same amplitude. In reality, their relative intensities roughly increase with increasing Mn-concentration. However, we observed deviations from a simple proportionality, which can be ascribed to different degrees of implantation for the five samples. The EPR spectra are typical for exchange-coupled Mn^{2+} ions in (Cd,Mn) and (Zn,Mn) chalcogenide mixed crystals [11–13]. The features in the EPR spectra can be best explained in the spectrum of the $x = 1.5\%$ sample. This spectrum consists of a sextet of sharp lines, each line with a pair of satellites at lower magnetic field on a broad background. The g-factor is 2.001. The sharp lines and their satellites correspond to the "allowed" ($\Delta m_S = \pm 1, \Delta m_I = 0$) and the "forbidden" ($\Delta m_S = \pm 1, \Delta m_I = \pm 1$) hyperfine transitions of the Zeeman-splitted $m_S = -1/2$ and $m_S = +1/2$ levels of the $^6S_{5/2}$ (or $^6A_1$) ground state of the Mn^{2+} 3d-electrons. The hyperfine structure arises from the interaction between the $S = 5/2$ spin of the unpaired

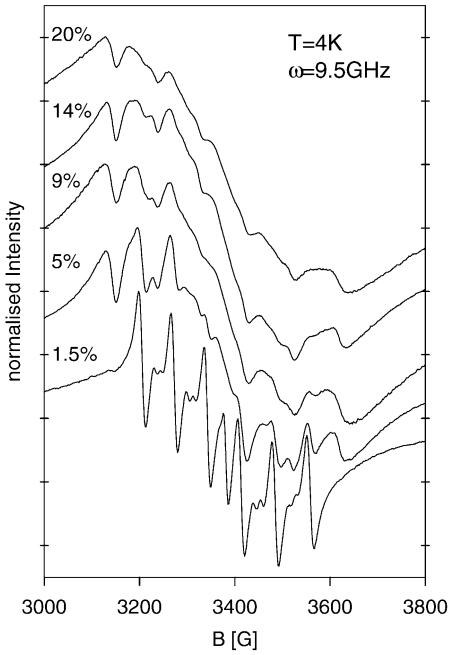

Fig. 2. Normalized EPR spectra of five $Cd_{1-x}Mn_xS$ in mesoporous MCM-41 SiO_2 samples of different Mn-contents x. At $T = 4$ K using an X-band frequency of 9.48 GHz.

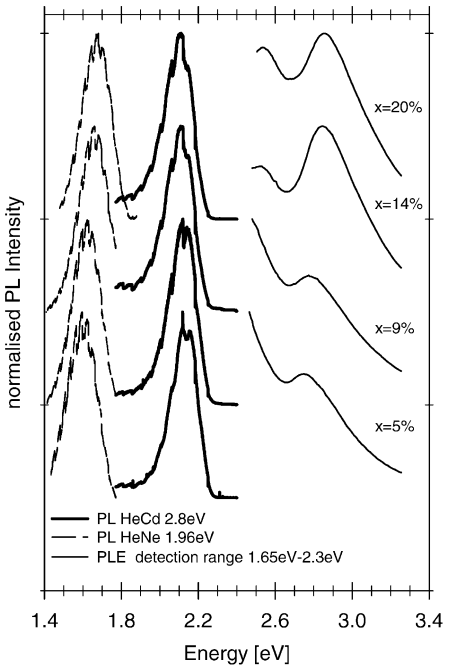

Fig. 3. Photoluminescence (PL) and PL excitation (PLE) spectra of four $Cd_{1-x}Mn_xS$ in mesoporous MCM-41 SiO_2 samples of different Mn-contents x. The PL spectra were taken at $T = 2$ K using two different excitation energies. The PLE spectra were taken at $T = 10$ K using the "yellow" PL band for detection.

3d-electrons and the $I = 5/2$ spin of the Mn^{2+} nucleus. The $\Delta m_S = \pm 1$ transition energies between the Zeeman levels $m_S = \pm 5/2$ and $m_S = \pm 3/2$ as well as $m_S = \pm 3/2$ and $m_S = \pm 1/2$ vary with changing crystal orientation in the range of about 20 G with respect to the $m_S = -1/2$ to $m_S = +1/2$ transitions [11]. Therefore, the corresponding sextets of lines cannot be distinguished in the spectrum of powdered samples, but their averaging determines the width of the six resonance lines. The spectrum of $x = 1.5\%$ is typical for Mn^{2+} ions in the tetrahedral environment of a Cd-site in a zincblende crystal [11,14]. Thus, the crystal structure of the $Cd_{0.985}Mn_{0.015}S$ wires is probably zincblende, which is often found for CdS nanoclusters containing only little manganese [14]. With increasing x the structures are smeared out due to the increasing superexchange interaction between the Mn^{2+} ions [15,16]. In addition, the broad background strongly increases and the "forbidden" hyperfine transitions become more prominent for $x \geqslant 5\%$. These are typical features of Mn^{2+} on a Cd-site in a wurtzite crystal [13,15], which is also tetrahedrally coordinated, but with a strong tetragonal distortion. Such a tetragonal distortion gives rise to a much stronger crystal-field splitting of the Mn^{2+} ground state compared to that in a zincblende structure. Due to the stronger crystal field the orientation dependent EPR spectrum in wurtzite extends over a field range of about 1500 G [11]. In the powder average this yields a broad resonance line with a width of some 100 G. The observed differences between the EPR spectra for $x = 1.5\%$ and $x \geqslant 5\%$ agree well with the assumption that the crystal structure of the $Cd_{1-x}Mn_xS$ nanowires changes with increasing x from zincblende to wurtzite.

Fig. 3 depicts PL and PLE spectra of the four wurtzite $Cd_{1-x}Mn_xS$ quantum wire samples with $x = 5\%$, 9%, 14% and 20%. The PL spectra were taken at 2 K using two different excitation energies. For excitation above or close to the bandgap, using the 441 nm (2.81 eV) or the 325 nm (3.81 eV) line of the HeCd laser, the PL is dominated by the yellow luminescence band at about 2.1 eV. This PL band originates from the 3d-internal transition of Mn^{2+} on

a Cd-site. The transition takes place between the $^4T_1$ first excited state and the $^6A_1$ ground state. Due to the efficient energy transfer from the $Cd_{1-x}Mn_xS$ band states into the Mn^{2+}-subsystem, there is no band-gap related excitonic PL in the cw measurement. Using a laser excitation energetically below the yellow PL band, another red PL band centred at 1.52 eV is excited. It originates from the 3d-internal transition of another Mn^{2+}-related defect which has either tetrahedral site symmetry but with a different crystal field or corresponds to a site with octahedral symmetry. These PL bands are typical for (Cd,Mn) and (Zn,Mn) chalcogenide mixed crystals [17–19].

The PLE spectra in Fig. 3 were taken at 10 K using the yellow PL band in the range from 1.65 to 2.4 eV. All four spectra show a distinct peak followed by an increase in intensity at lower energies. This increase in intensity is related to the high energy shoulder of the $^6A_1 \rightarrow ^4T_1$ absorption within the 3d-shell of Mn^{2+} on a Cd-site [18,19]. The energy position of the peak in the PLE spectra varies strongly with Mn-concentration. Therefore, this feature corresponds to the band gap absorption of the $Cd_{1-x}Mn_xS$ quantum wires as the energy positions of Mn-internal absorption bands are to a good approximation independent of Mn^{2+}-concentration [17]. The signal strength of the $Cd_{1-x}Mn_xS$ band gap feature reflects again the efficient energy transfer from the band states into the Mn^{2+}-subsystem pointed out in the discussion of the PL bands.

The inset of Fig. 4 shows the s, p–d exchange induced splitting for σ^+ and σ^--polarisation of the PLE band corresponding to the bandgap of the $Cd_{0.86}Mn_{0.14}S$ quantum wire sample in a magnetic field. The spectra were taken in Faraday geometry at $T = 2$ K and $B = 7.5$ T. At first sight, the observed splitting of only about 40 meV appears to be relatively small for (Cd,Mn) and (Zn,Mn) chalcogenide mixed crystals, in particular, for $Cd_{1-x}Mn_xS$, which is supposed to have very large exchange integrals $N_0\alpha$ and $N_0\beta$ [17]. The reason for the small observed splitting is that the polarisation information of the excitation light is partly lost in scattering and refraction processes at the interfaces of different powder grains, which occur before the absorption leading to the PLE emission.

Fig. 4 shows a comparison of the band gap energies obtained from the PLE spectra in Fig. 3 with

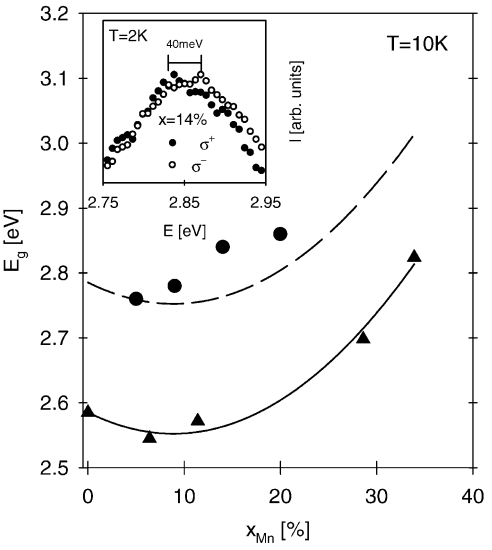

Fig. 4. Comparison of the band gap variation with x for $Cd_{1-x}Mn_xS$ in mesoporous MCM-41 SiO_2 quantum wires (full circles) and bulk $Cd_{1-x}Mn_xS$ (full triangles) given in Ref. [20]. $T = 10$ K. The solid line and the dashed line are guides to the eye. Inset: s, p–d exchange induced energy splitting of the bandgap of the $Cd_{0.86}Mn_{0.14}S$ quantum wire sample observed in Faraday geometry at $T = 2$ K and at $B = 7.5$ T.

those of bulk $Cd_{1-x}Mn_xS$ given in Ref. [20]. The solid line is a guide to the eye representing the p–d exchange-induced band gap bowing of (Cd,Mn)S [21]. The dashed line represents a shift of the solid line by 200 meV. All the band gap data of the $Cd_{1-x}Mn_xS$ quantum wires are above the dashed line showing that the quantum confinement energy in the wires is more than 200 meV. Such large values for the quantum confinement are expected for wires with lateral dimensions of only 3.1 nm. Similar confinement energies have been observed for $Cd_{1-x}Mn_xS$ nanoparticles of comparable sizes [22]. An increasing deviation from the dashed line with increasing x of the experimental data for the quantum wires is observed as a trend, also in good agreement with previous studies [22]. A possible explanation for this trend is an enhancement of the p–d exchange interaction caused by modified positions of the p-and d-related bands in the bandstructure of the quantum wires compared to bulk. Due to the quantum confinement, the lowest valence band state of the $Cd_{1-x}Mn_xS$ quantum wires is shifted significantly towards the Mn 3d states, which are positioned

about 3 eV below the valence band edge of bulk material. This enhancement effect is similar to that in bulk $Cd_{1-x}Mn_xY$ with Y=Te, Se, S where an increased p–d hybridisation is observed with increasing band gap on going from Te to S [23].

4. Conclusions

To summarise, we have demonstrated that highly ordered arrays of magnetic quantum wires can be obtained by incorporating the semimagnetic semiconductor $Cd_{1-x}Mn_xS$ into the regular pores of hexagonal MCM-41 SiO_2. The crystal structure of the $Cd_{1-x}Mn_xS$ quantum wires changes with increasing x from zincblende to wurtzite. Comparing the energy positions of the bandgaps of the wurtzite $Cd_{1-x}Mn_xS$ wires with those of wurtzite bulk samples yields a quantum confinement of about 200 meV in our structures. The photoluminescence of the wires as in bulk $Cd_{1-x}Mn_xS$ is dominated by the 3d-internal emission of the Mn^{2+} ions.

Highly ordered mesoporous inorganic structures synthesised by organic-template directed pathways will offer possibilities for constructing regular semiconductor structures on length scales not accessible by standard lithography methods. Therefore, these growth techniques might be of interest for a further miniaturisation of standard electronic and magneto-electronic devices.

Acknowledgements

Funding by the Deutsche Forschungsgemeinschaft (Grants Fr 1372/4-1 and He 2298/4-1) and the Fonds der Chemischen Industrie is gratefully acknowledged.

References

[1] C.T. Kresge, M.E. Leonowicz, W.J. Roth, J.C. Vartuli, J.S. Beck, Nature 359 (1992) 710.
[2] Q. Huo, D.I. Margolese, U. Ciesla, P. Feng, T.E. Gier, P. Sieger, R. Leon, P.M. Petroff, F. Schüth, G.D. Stucky, Nature 368 (1994) 317.
[3] M. Thommes, R. Köhn, M. Fröba, J. Phys. Chem. B 104 (2000) 7932.
[4] T. Hirai, H. Okubo, I. Komasawa, J. Phys. Chem. B 103 (1999) 4228.
[5] H. Parala, H. Winkler, M. Kolbe, A. Wohlfahrt, R.A. Fischer, R. Schmechel, H. von Seggern, Adv. Mater. 12 (2000) 1050.
[6] V.I. Srdanov, I. Alxneit, G.D. Stucky, C.M. Reaves, S.P. DenBaars, J. Phys. Chem. B 102 (1998) 3341.
[7] J.R. Agger, M.W. Anderson, M.E. Pemble, O. Terasaki, Y. Nozue, J. Phys. Chem. B 102 (1998) 3345.
[8] R. Leon, D. Margolese, G. Stucky, P.M. Petroff, Phys. Rev. B 52 (1995) R2285.
[9] Y.S. Tang, S. Cai, G. Jin, J. Duan, K.L. Wang, H.M. Soyez, B.S. Dunn, Appl. Phys. Lett. 71 (1997) 2449.
[10] L. Chen, P.J. Klar, W. Heimbrodt, F. Brieler, M. Fröba, Appl. Phys. Lett. 76 (2000) 3531.
[11] J. Schneider, S.R. Sircar, A. Räuber, Z. Naturforschg. 18a (1963) 980.
[12] J. Lambe, C. Kikuchi, Phys. Rev. 119 (1960) 1256.
[13] Y. Ishikawa, J. Phys. Soc. Jpn. 21 (1966) 1473.
[14] D.M. Hofmann, A. Hofstaetter, U. Leib, B.K. Meyer, C. Counio, J. Crystal Growth 184–185 (1998) 383.
[15] N. Samarth, J.K. Furdyna, Phys. Rev. B 37 (1988) 9227.
[16] O. Goede, D. Backs, W. Heimbrodt, M. Kanis, Phys. Stat. Sol. (b) 151 (1989) 311.
[17] O. Goede, W. Heimbrodt, Phys. Stat. Sol. (b) 146 (1988) 11.
[18] O. Goede, W. Heimbrodt, V. Weinhold, Phys. Stat. Sol. (b) 136 (1986) K49.
[19] W. Heimbrodt, C. Benecke, O. Goede, H.-E. Gumlich, Phys. Stat. Sol. (b) 154 (1989) 405.
[20] C.T. Tsai, S.H. Chen, D.S. Chuu, W.C. Chou, Phys. Rev. B 54 (1996) 11555.
[21] R.B. Bylsma, W.M. Becker, J. Kossut, U. Debska, Phys. Rev. B 33 (1986) 8207.
[22] L. Levy, N. Feltin, D. Ingert, M.P. Pileni, J. Phys. Chem. B 101 (1997) 9153.
[23] M. Taniguchi, M. Fujimori, M. Fujisawa, T. Mori, I. Souma, Y. Oka, Solid State Commun. 62 (1987) 431.